The Geometry of Far-Field Passive Source Localization with TDOA and FDOA

Karleigh Cameron Pine, Samuel Pine, and Margaret Cheney, *Senior Member, IEEE*

***Abstract*—Passive localization of acoustic or radio-frequency sources is often performed using time difference of arrival (TDOA) measurements and/or frequency difference of arrival (FDOA) measurements. TDOA localization has been thoroughly studied, but FDOA less so. This is largely because the TDOA level surfaces are hyperboloids, which are well-understood, whereas the FDOA level curves and surfaces are much more complicated. This paper addresses the case of known sensor positions and velocities and a stationary source. The paper shows examples of the FDOA level curves and surfaces, and shows that they simplify dramatically in the far field, *i.e.*, when the source is much farther from the origin than are the sensors. The far-field behavior is of two types, depending on whether the sensor velocities are equal or unequal. The far-field behavior gives insight into conditions needed for far-field TDOA-FDOA localization and FDOA-only localization. The paper includes a characterization of feasible far-field TDOA and unequal-velocity FDOA data.**

***Index Terms*—source localization, TDOA, FDOA, Doppler, DOA, far-field**

I. Introduction

The problem of locating a source of acoustic or radio-frequency energy is a problem that arises in many applications. There are four main classes of approaches:

1) Triangulation. Use multiple spatially separated receiver arrays, determine the direction of arrival (DOA) from each, and triangulate to locate the source;
2) Two-step methods. From spatially separated, clock-synchronized receivers, compute the time difference of arrival (TDOA) and/or frequency difference of arrival (FDOA) between those receivers, and solve polynomial equations to locate the source (e.g., [1], [2], [3], [4], [5]);
3) Direct position determination. From spatially separated, clock-synchronized receivers, first estimate the transmitted waveform and then plot or maximize the likelihood function as a function of source position (e.g., [6], [7], [8];
4) Synthetic-aperture source localization. From clock-synchronized receivers with different trajectories, use a synthetic-aperture approach to form an image of source locations [7], [9], [10].

The triangulation approach 1) has the advantage of not requiring temporal coherence between spatially separated receivers, but it is known to provide only coarse spatial resolution. The other three approaches all use cross-correlations or cross-ambiguity functions in somewhat different ways, and are thus implicitly making use of TDOA and/or FDOA information. This means that an analysis of the geometrical constraints imposed by TDOA and FDOA data can contribute to our understanding of the performance of methods 2)-4).

The geometry associated with TDOA measurements is well-understood (e.g., [4], [5], [11], [12], [13], [14], [15]). Geometrically, each TDOA measurement restricts the possible transmitter locations to a hyperboloid. Thus, if several TDOA measurements are obtained, locating the emitter effectively requires finding the intersection of several hyperboloids.

When the distance between the receivers and the transmitter is much greater than the distance between the receivers, wavefront curvature is negligible in the region of the receivers. This assumption is commonly referred to as the far-field assumption [16]. It is well-known that the TDOA equations become linear in the far field [14] and this dramatically simplifies TDOA analysis in the far field.

The geometry associated with FDOA measurements is much less well-understood. Analysis of the FDOA contributions to source localization has mainly been through the study of Cramèr-Rao bounds (e.g., [3], [17]) but the results have not been interpreted in terms of geometry. Although a few incidental plots of some FDOA level curves have appeared in the literature (e.g., [9], [18], [19], [20]), no systematic study of the FDOA geometry has been published. This is because the FDOA level surfaces or iso-surfaces (*i.e.,* the set of points in space that give rise to a certain FDOA) are much more complicated than the TDOA hyperboloids. The FDOA equations can be converted to a polynomial system [5], but this system has degree 8, and consequently its study is quite difficult.

In this paper we show examples of some of the FDOA level curves and surfaces. We make some basic observations about the FDOA equations, in particular showing that in the far field, the FDOA geometry simplifies dramatically. Although this simple observation requires little mathematical machinery, it does not seem have been noted in the literature, and it has some interesting consequences that are discussed in this paper.

We give explicit closed-form expressions for the far-field FDOA surfaces and find that there are two types of behavior, depending on the relationship between the sensor velocities. For the simpler unequal-velocity case, we show that:

1) far-field FDOA measurements provide DOA information only;
2) the far-field DOA information obtained from FDOA is the

Manuscript received January 1, 2021; revised March 2021.

K.C. Pine and S. Pine are with Matrix Research, Inc.; M. Cheney is with Colorado State University.

This material is based upon work supported by the Air Force Office of Scientific Research under award number FA9550-18-1-0087 and by the Office of Naval Research under award number N00014-21-1-2145 and under the Faculty Sabbatical program.

same as that obtained from TDOA;
3) with the additional constraint that the source lies on a known surface not containing the sensors ("altitude constraint"), there can be a quasi-near-field region in which FDOA and TDOA information is independent.
In particular, conclusion 2) may explain the poor far-field performance of some TDOA-FDOA localization results (e.g. [21]).

In addition, we
4) give a characterization of the possible far-field TDOA and FDOA measurements from multiple sensors; and
5) observe that the explicit pseudo-inverse formula for the DOA from far-field data incorporates automatic de-noising in the sense that the formula involves a projection onto the feasible measurement space.

These geometrical observations 1)-3) and associated conclusions 4)-5) are all simple but do not seem to appear anywhere in the literature.

The paper is organized as follows. In section II we define the TDOA and FDOA and show examples of their level curves and surfaces. In section III we note basic properties of the FDOA, including its sensitivity to source position and its two far-field simplifications. In section IV we study far-field TDOA-FDOA localization, and discover that without constraints, the DOA information obtained from TDOA and FDOA are the same, but that with an "altitude constraint", there is an interesting quasi-near-field region in which TDOA and FDOA information can be combined to provide range information. In section V we characterize the feasible TDOA and FDOA far-field measurements. In section VI we summarize the findings. Finally, two appendices show the details of some of the results used in the text.

II. TDOA and FDOA Measurements

In this section, we establish the definitions and notation for TDOA and FDOA, and show examples of some FDOA level curves and surfaces.

An acoustic or electromagnetic wave propagating from a source at $\boldsymbol{y} \in \mathbb{R}^3$ to a receiver at $\boldsymbol{x} \in \mathbb{R}^3$, in a homogeneous medium with wave speed c, undergoes a time delay $R_{\boldsymbol{x},\boldsymbol{y}}/c$, where $R_{\boldsymbol{x},\boldsymbol{y}} = \|\boldsymbol{x}-\boldsymbol{y}\|$. Here $\|\cdot\|$ denotes the usual Euclidean distance. We denote by τ the time delay multiplied by c, so that $\tau(\boldsymbol{x},\boldsymbol{y}) = R_{\boldsymbol{x},\boldsymbol{y}}$. When there is relative motion between the transmitter at $\boldsymbol{y}$ and the receiver at $\boldsymbol{x}$, the frequency of the arriving signal is $\nu_0(1 - \widehat{\boldsymbol{R}}_{\boldsymbol{x},\boldsymbol{y}} \cdot \boldsymbol{v}/c)$, where $\boldsymbol{v}$ is the relative velocity, where ν_0 is the transmitting frequency, and where $\widehat{\boldsymbol{R}}_{\boldsymbol{x},\boldsymbol{y}} = \boldsymbol{R}_{\boldsymbol{x},\boldsymbol{y}}/R_{\boldsymbol{x},\boldsymbol{y}}$ with $\boldsymbol{R}_{\boldsymbol{x},\boldsymbol{y}} = \boldsymbol{x} - \boldsymbol{y}$. Below we also use the simplified notation $\boldsymbol{R}_{\boldsymbol{y},i} \doteq \boldsymbol{R}_{\boldsymbol{y},\boldsymbol{x}_i}$.

Because we do not know the transmit time or frequency, measurement of the arrival time and/or measured frequency of a signal does not help us locate the source from a single sensor. However, the *difference* of these quantities, measured at pairs of receivers, provides information that can be used to locate the source.

In practice, the time delay, known as the Time Difference of Arrival (TDOA), and the difference of Doppler factors, known as the Frequency Difference of Arrival (FDOA) or differential Doppler, can be obtained from a cross-ambiguity function or coherence function of signals measured at two receivers. The TDOA and FDOA also appear as the focusing conditions in a synthetic-aperture approach [10].

In the following, we assume that processing has been done in such a way (perhaps by taking quotients of measured frequencies) so that the transmit frequency has cancelled out, and the FDOA involves no unknown transmit frequency.

In this paper, we consider a single stationary transmitter located at $\boldsymbol{y}$, and n receivers located at $\boldsymbol{x}_1, ..., \boldsymbol{x}_n$ with velocities $\boldsymbol{v}_1, ..., \boldsymbol{v}_n$. We write $\tau_i = \tau(\boldsymbol{y}, \boldsymbol{x}_i)$ etc. When all the velocities are the same, the theory also applies to the case of fixed receivers and a moving source with known velocity.

A. Time Difference of Arrival (TDOA)

The time difference of arrival from a signal transmitted at $\boldsymbol{y}$ to sensors at $\boldsymbol{x}_i$ and $\boldsymbol{x}_j$ is

$$\tau_{i,j} \doteq \tau_i - \tau_j = \|\boldsymbol{y} - \boldsymbol{x}_i\| - \|\boldsymbol{y} - \boldsymbol{x}_j\|. \tag{1}$$

In free space, the iso-TDOA surfaces, *i.e.* the set of $\boldsymbol{y}$ for which $\tau_{i,j}$ is constant, are hyperboloids. If $\boldsymbol{x}_i, \boldsymbol{x}_j$, and $\boldsymbol{y}$ are all on the same plane, these level curves are hyperbolas [22]. Examples are shown in Fig. 1 for $\boldsymbol{x}_1 = (1,0), \boldsymbol{x}_2 = (-1,0)$. It is well-known that far from the origin, hyperbolas are

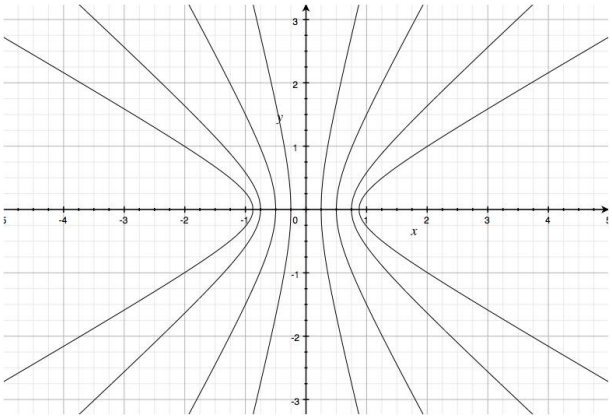

Fig. 1. Iso-TDOA curves for sensor positions $\boldsymbol{x}_1 = (1,0), \boldsymbol{x}_2 = (-1,0)$. Iso-TDOA surfaces are obtained by revolving this figure about the horizontal axis.

asymptotic to straight lines through the origin. These lines give the DOA of the source at $\boldsymbol{y}$. In three dimensions, the far-field iso-TDOA surfaces are asymptotic to cones whose axis is the sensor axis.

To determine equations for these asymptotic lines and cones, we use the far-field approximation, which applies when all the receivers are much closer to the origin than is the emitter, *i.e.,* $\|\boldsymbol{x}_i\| \ll \|\boldsymbol{y}\|$ for all i. Using this assumption to expand the square root leads to (see, e.g., [16])

$$R_{\boldsymbol{y},i} \doteq \|\boldsymbol{y} - \boldsymbol{x}_i\| = \|\boldsymbol{y}\| - \widehat{\boldsymbol{y}}^T \cdot \boldsymbol{x}_i + \mathcal{O}\left(\frac{\|\boldsymbol{x}_i\|}{\|\boldsymbol{y}\|}\right) \tag{2}$$

where the T denotes transpose and the hat denotes unit vector. The use of (2) in (1) leads to the equation for the TDOA far-field approximation:

$$\tau_{i,j} \approx -\widehat{\boldsymbol{y}}^T \cdot (\boldsymbol{x}_i - \boldsymbol{x}_j). \tag{3}$$

The set of points $\boldsymbol{y}$ for which (3) is constant is a cone whose axis is $\boldsymbol{x}_i - \boldsymbol{x}_j$ and whose vertex is at the origin.

B. Frequency Difference of Arrival (FDOA)

The Doppler factor for the signal between the emitter at $\boldsymbol{y}$ and the i^{th} receiver is proportional to

$$d_i \doteq \boldsymbol{v}_i^T \cdot \widehat{\boldsymbol{R}}_{\boldsymbol{y},i}, \tag{4}$$

where again T denotes transpose and the hat denotes unit vector.

The FDOA is defined here as

$$f_{i,j} \doteq d_i - d_j = \boldsymbol{v}_i^T \cdot \widehat{\boldsymbol{R}}_{\boldsymbol{y},i} - \boldsymbol{v}_j^T \cdot \widehat{\boldsymbol{R}}_{\boldsymbol{y},j}. \tag{5}$$

One simple special case is when one of the velocities is zero; this FDOA iso-surface is simply a cone whose axis is the nonzero velocity. When both velocities are nonzero, the surfaces of constant $f_{i,j}$ are much more difficult to describe. Examples of planar FDOA iso-curves, for a variety of different unequal velocity choices, are shown in Fig. 2. Examples of FDOA iso-surfaces are shown in Fig. 3. The middle plot of Fig. 3 shows singularities (the tips of the "horns") at the sensor positions.

The complexity of the near-field FDOA curves and surfaces suggests that linearization approaches such as those of [23] are likely to be useful only when there is very good prior information about the source location. The reader is invited to consider the consequences of the FDOA geometry for a) any source localization method involving the intersection of one of the TDOA curves of Fig. 1 with one of the FDOA curves in Fig. 2, or b) an FDOA-only source localization method that would involve intersections of one curve of Fig. 2 with a second such curve that has been rotated and translated so that it corresponds to different sensor locations.

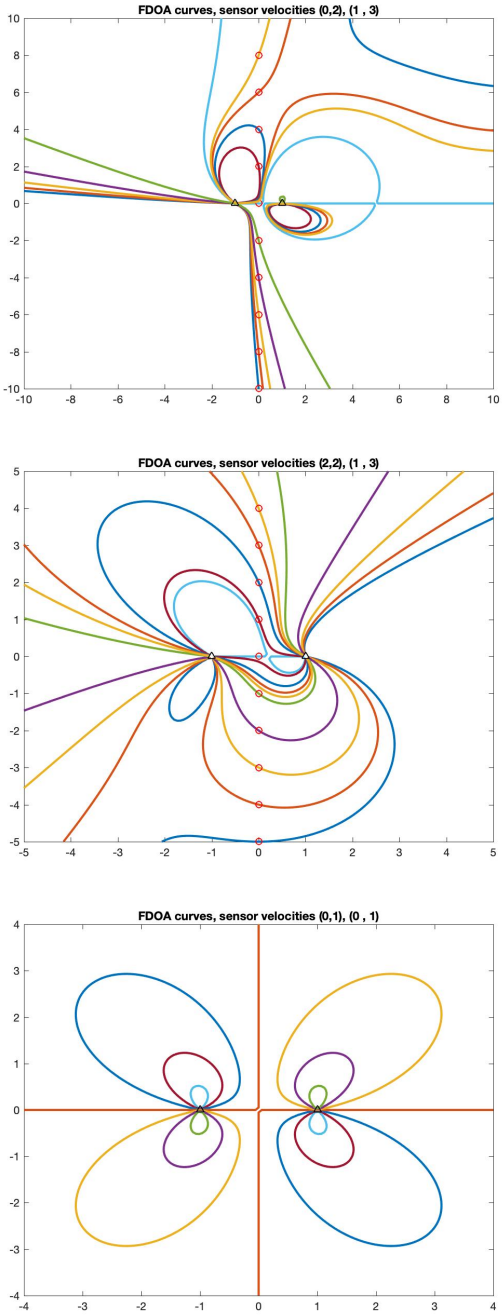

Fig. 2. Examples of near-field FDOA iso-curves (4) for sensors located at $(1, 0)$ and $(-1, 0)$, for a variety of sensor velocity choices. The bottom plot shows the case in which both sensors have the same velocity along the y-axis. In the top two plots, the curves were chosen to pass through the small red circles; the bottom plot shows curves for equally spaced values of the FDOA.

III. Properties of the FDOA

In this section, we establish the sensitivity of the FDOA to source position (section III-A) and simplified far-field formulas for the FDOA (section III-B).

The FDOA has received much less study than has the TDOA. Some basic properties of the FDOA are the following.

A. Sensitivity of FDOA to source position

The derivative of FDOA with respect to source position is

$$\nabla_{\boldsymbol{y}} f_{i,j} = \frac{I - \widehat{\boldsymbol{R}}_{\boldsymbol{y},i}\widehat{\boldsymbol{R}}_{\boldsymbol{y},i}^T}{\|\boldsymbol{R}_{\boldsymbol{y},i}\|} \cdot \boldsymbol{v}_i - \frac{I - \widehat{\boldsymbol{R}}_{\boldsymbol{y},j}\widehat{\boldsymbol{R}}_{\boldsymbol{y},j}^T}{\|\boldsymbol{R}_{\boldsymbol{y},j}\|} \cdot \boldsymbol{v}_j \tag{6}$$

(see Appendix A.) This shows that when the source at $\boldsymbol{y}$ recedes from both sensors, changes in the position $\boldsymbol{y}$ cause smaller and smaller changes in the FDOA. In other words, determining source position from the FDOA becomes increasingly ill-posed at larger distances.

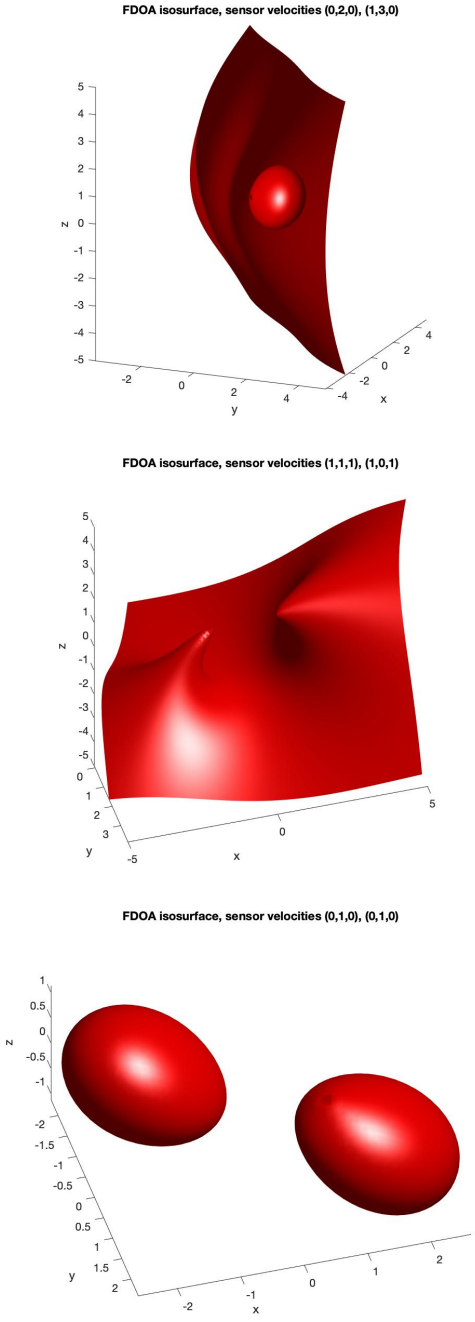

Fig. 3. Examples of near-field FDOA iso-surfaces (4) for sensors located at $(1,0)$ and $(-1,0)$, for a variety of sensor velocity choices. These surfaces were chosen to pass through the (near-field) point $(1,1,1)$. The top two plots involve unequal velocities, whereas the bottom plot shows the case with extra symmetry, in which both sensors have the same velocity along the y-axis.

B. Far-field FDOA formulas

Following [24], we consider the far-field FDOA case, where all the receivers are much closer to the origin than is the emitter, *i.e.,* where $\|\boldsymbol{x}_i\| \ll \|\boldsymbol{y}\|$. We use just the first term of (2) in the denominator of $\widehat{\boldsymbol{R}}$ to obtain

$$\widehat{\boldsymbol{R}}_{\boldsymbol{y},i} = \frac{\boldsymbol{R}_{\boldsymbol{y},i}}{R_{\boldsymbol{y},i}} = \frac{\boldsymbol{x}_i - \boldsymbol{y}}{\|\boldsymbol{x}_i - \boldsymbol{y}\|} \approx \frac{\boldsymbol{x}_i}{\|\boldsymbol{y}\|} - \frac{\boldsymbol{y}}{\|\boldsymbol{y}\|} \approx -\widehat{\boldsymbol{y}}, \quad (7)$$

where $-\widehat{\boldsymbol{y}} = -\boldsymbol{y}/\|\boldsymbol{y}\|$.

Consequently, the far-field expression for the FDOA is

$$f_{i,j} \approx (\boldsymbol{v}_i - \boldsymbol{v}_j)^T \cdot \widehat{\boldsymbol{y}}. \quad (8)$$

When $\boldsymbol{v}_i \neq \boldsymbol{v}_j$, the set of points $\boldsymbol{y}$ for which (8) is constant is a cone whose axis is $\boldsymbol{v}_i - \boldsymbol{v}_j$ and whose vertex is at the origin. The top plot of Fig. 5 shows a typical example. If the sensors, velocities, and source are all co-planar, then the FDOA iso-curve consists of two lines through the origin, one of which gives the DOA. The top plot of Fig. 4 shows a typical two-dimensional example of this linear behavior of the FDOA iso-curves in the far field.

The case of identical velocities is important because it corresponds to the case of fixed sensors and a moving source. In the equal-velocity case, the leading-order term (8) vanishes, and (5) can be written as

$$f_{i,j} = \boldsymbol{v}^T \cdot \left(\widehat{\boldsymbol{R}}_{\boldsymbol{y},i} - \widehat{\boldsymbol{R}}_{\boldsymbol{y},j}\right). \quad (9)$$

In this case, we approximate the difference in unit vectors by the derivative (see Appendix A) evaluated at the midpoint $\boldsymbol{x}_{ij}$ between $\boldsymbol{x}_i$ and $\boldsymbol{x}_j$. We thus obtain the far-field expression

$$f_{i,j} = \boldsymbol{v}^T \cdot \frac{I - \widehat{\boldsymbol{R}}_{\boldsymbol{y}}\widehat{\boldsymbol{R}}_{\boldsymbol{y}}^T}{\|\boldsymbol{R}_{\boldsymbol{y}}\|} \cdot (\boldsymbol{x}_i - \boldsymbol{x}_j), \quad (10)$$

where $\boldsymbol{R}_{\boldsymbol{y}} = \boldsymbol{y} - \boldsymbol{x}_{ij}$. When the sensors are symmetric with respect to the origin, the midpoint $\boldsymbol{x}_{ij}$ is the origin, and $\boldsymbol{R}_{\boldsymbol{y}}$ is simply $\boldsymbol{y}$.

To plot iso-surfaces of (10), we can rewrite (10) as

$$\|\boldsymbol{R}_{\boldsymbol{y}}\| = \frac{\boldsymbol{v}^T \cdot \left(I - \widehat{\boldsymbol{R}}_{\boldsymbol{y}}\widehat{\boldsymbol{R}}_{\boldsymbol{y}}^T\right) \cdot (\boldsymbol{x}_i - \boldsymbol{x}_j)}{f_{i,j}}, \quad (11)$$

which, with $f_{i,j}$ fixed, is a polar- or spherical-coordinate formula[1] giving the range $r = \|\boldsymbol{R}_{\boldsymbol{y}}\|$ in terms of the direction $\widehat{\boldsymbol{R}}_{\boldsymbol{y}}$. We note that the expression $I - \widehat{\boldsymbol{R}}_{\boldsymbol{y}}\widehat{\boldsymbol{R}}_{\boldsymbol{y}}^T$ in the numerator of (10) is a projection operator that projects a vector onto the plane perpendicular to the vector $\widehat{\boldsymbol{R}}_{\boldsymbol{y}}$. Thus the surface (11) passes through the origin when $\boldsymbol{y}$ is either in the direction of the sensor axis $(\boldsymbol{x}_i - \boldsymbol{x}_j)$ or in the direction of the velocity axis $\boldsymbol{v}$.

The middle plot of Fig. 4 shows some FDOA curves for the equal-velocity case; the bottom plot of Fig. 4 shows the corresponding plot produced from (11). The bottom plot of Fig. 5 shows a typical example of an equal-velocity far-field iso-suface.

[1]Note that not all combinations of $\boldsymbol{v}$, $\boldsymbol{x}_i - \boldsymbol{x}_j$, and $f_{i,j}$ result in a positive radius. This is connected to the question of which measurements $f_{i,j}$ are feasible.

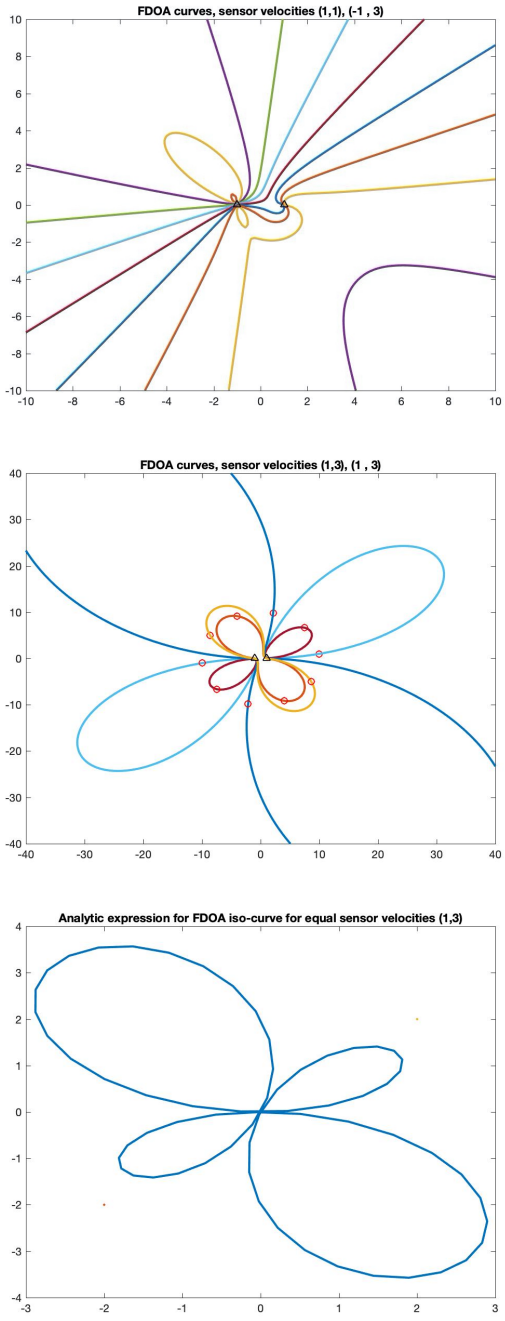

Fig. 4. The first figure shows a typical example of FDOA iso-curves for unequal velocities, with complicated curves in the near field that become lines in the far field. The second plot shows a variety of FDOA iso-curves, chosen to pass through the small red circles, for the case when both sensors have velocity $(1, 3)$. The bottom plot shows a plot produced from (11) for the same velocities as in the second plot. In all cases, the sensors are at $(1, 0)$ and $(-1, 0)$.

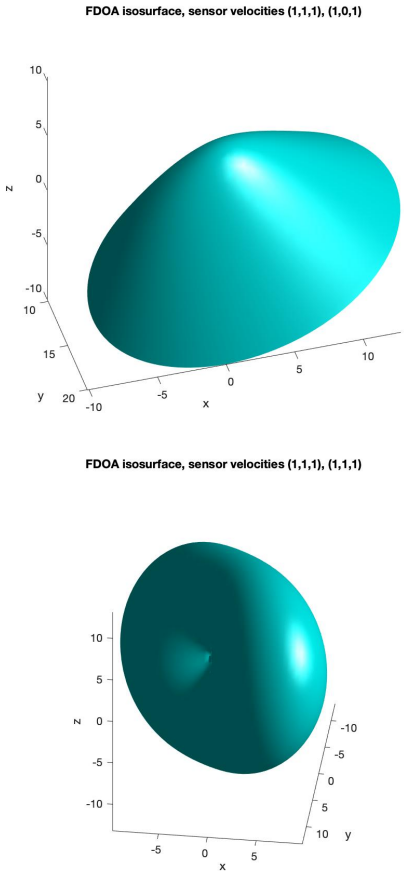

Fig. 5. The first figure shows a typical example of a far-field FDOA iso-surface for unequal velocities. The second plot shows a typical far-field equal-velocity case. Again the sensors are at $(1, 0)$ and $(-1, 0)$, and these surfaces pass through the (far-field) point $(1, 10, 0)$. The first plot shows the far-field case for parameters of the second plot of Fig. 3.

IV. Far-field TDOA-FDOA Localization

In this section, we analyze the geometry involved in TDOA-FDOA localization. We consider three cases: A) the purely two-dimensional case, B) the purely three-dimensional case, and C) the three-dimensional case in which the source is known to lie on a flat surface not containing the sensors.

From two sensors, one might hope to localize a single target on a known plane from simultaneous TDOA and FDOA measurements. It has been noted in the literature (*e.g.*, [25]) that this often works much better in the near field than in the far field, but this phenomenon does not seem to have been explained geometrically.

A. Two dimensions

For the case of different sensor velocities and a far-field source, the TDOA and FDOA information is not independent. This is because both the TDOA and FDOA curves are asymptotic to lines through the origin. Since these asymptotic lines pass through both the origin and the source, the TDOA and FDOA asymptotic lines coincide, and both provide only DOA information. A typical example is shown in the top plot of Fig. 6, where we see complicated behavior of the orange FDOA

curve near the origin, but linear behavior already for a source located at $(10, 10)$. The blue curve is the TDOA hyperbola.

The equal-velocity TDOA-FDOA case, however, is better; an example is shown in the middle plot in Fig. 6. The equal-velocity case allows far-field transverse intersections, provided the source is not close to the sensor axis or the velocity axis. FDOAs for sources in the degenerate directions (along the sensor axis or velocity axis) are again defined by the corresponding radial line, which is again tangent to the far-field TDOA curve. The bottom plot in Fig. 6 shows an example of the degenerate equal-velocity case with a source along the velocity axis.

B. Three dimensions

In the unequal-velocity three-dimensional case, the constant-TDOA far-field surface is a cone (3) with axis $\boldsymbol{x}_i - \boldsymbol{x}_j$, and the constant-FDOA far-field surface is a cone (8) with axis $\boldsymbol{v}_i - \boldsymbol{v}_j$. (See the top plot in Fig. 5.) These cones both have their vertices at the origin, and consequently both cones contain the line joining the origin to the source. Thus for a purely three-dimensional far-field problem, the TDOA and FDOA both provide information only about the DOA of the source and not its range.

Again, the equal-velocity case is better: a typical example of an equal-velocity FDOA surface is shown in the bottom plot of Fig. 5. The intersection of such a surface with a constant-TDOA cone is generally a closed curve in space. More information (such as a TDOA or FDOA from another sensor pair) is needed to determine the specific source location on this curve.

C. Three dimensions with known altitude

The situation changes somewhat when the source is known to lie on a surface, say a flat horizontal plane $y_3 = h$ that does not contain the sensors, which are assumed to lie near the origin. If the sensor axis and velocity axis are roughly horizontal, then the far-field TDOA and (unequal-velocity) FDOA cones both intersect the flat plane in hyperbolas (shown as dotted curves in Fig. 7). If the projection of the sensor midpoint is chosen to be the origin, then the hyperbolas are centered at $(0, 0, h)$, and in general their foci are at a distance of approximately $|h|$ from $(0, 0, h)$. (See Appendix B.) Thus, for an altitude significantly greater than the inter-sensor distance, the known-altitude configuration effectively produces a quasi-near-field region on the plane that extends to a distance comparable to the sensor height. In this quasi-near-field region, the FDOA iso-curves are simply hyperbolas, which are much simpler than the near-field FDOA iso-curves of a purely two-dimensional configuration. In this quasi-near-field region, the FDOA hyperbolas and TDOA hyperbolas intersect transversally, provided the respective cone axes (namely $\boldsymbol{v}_1 - \boldsymbol{v}_2$ and $\boldsymbol{x}_1 - \boldsymbol{x}_2$) are different.

The asymptotes of the hyperbolas on the plane are lines joining $(0, 0, h)$ to the source, and consequently, for sources located at distances much greater than $|h|$ from $(0, 0, h)$, the TDOA and (unequal-velocity) FDOA hyperbolas are again approximately tangent.

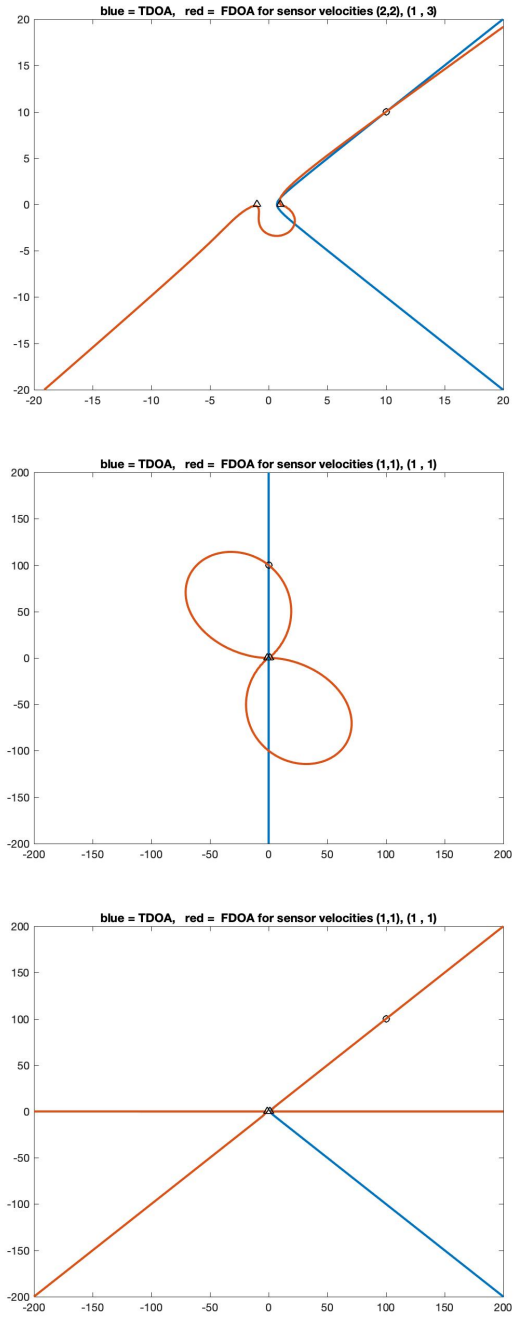

Fig. 6. Intersection of TDOA and FDOA curves for a source located at the small red circle. The red curve is the FDOA curve, and the blue curve is the TDOA hyperbola. The first plot shows a typical case of unequal velocities; the second shows an equal-velocity case in which the source is well away from both the sensor axis and the velocity axis; the bottom plot shows an equal-velocity degenerate case in which the source is aligned with the velocity axis.

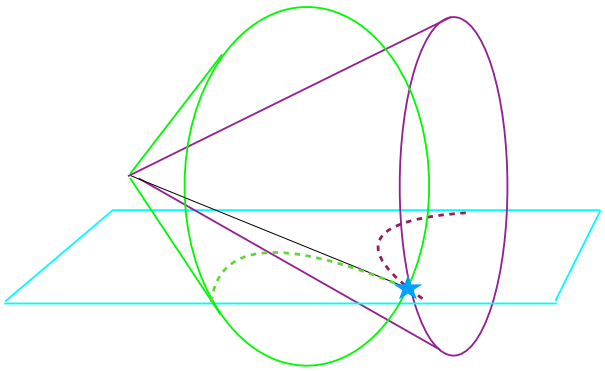

Fig. 7. TDOA and FDOA far-field cones with different cone axes, for a source known to lie somewhere on the horizontal plane. The intersection of the TDOA and FDOA hyperbolas (given by dashed lines) occurs at the source location, shown as a blue star.

Again the equal-velocity FDOA case is better, allowing transverse intersections of TDOA and FDOA surfaces at great distances from the sensors.

V. Feasible Far-field Measurements

In this section we address the question of which sets of TDOA and FDOA measurements can arise from a source in the far field.

Characterization of feasible far-field measurements may be useful for determining whether a source is, in fact, located far from the sensors. In addition, an understanding of the feasible far-field TDOA and FDOA measurements is potentially useful for noise suppression. In particular, one method for de-noising in TDOA-based geolocation is to project the noisy measurements onto the feasible set [12], [5], [24], [26]. This ensures that the TDOA measurements are physically realizable and consistent between receivers by enforcing a "closed loop" condition. We note below that in the far-field case, a similar approach applies to the unequal-velocity FDOA measurements.

The far-field TDOA approximation (3) can be assembled into the matrix form

$$\boldsymbol{\tau} = -\boldsymbol{P}\boldsymbol{X}\hat{\boldsymbol{y}}, \tag{12}$$

where each row of the matrix $\boldsymbol{X}$ is a receiver location, and $\boldsymbol{P}$ is a differencing matrix. For example, with 3 sensors, we can write the equations for the TDOA measurements $(\tau_{1,2}, \tau_{1,3})$ as

$$\boldsymbol{\tau} = \begin{pmatrix} \tau_{1,2} \\ \tau_{1,3} \end{pmatrix} = \underbrace{\begin{pmatrix} -1 & 1 & 0 \\ -1 & 0 & 1 \end{pmatrix}}_{-\boldsymbol{P}} \begin{pmatrix} \boldsymbol{x}_1^T \\ \boldsymbol{x}_2^T \\ \boldsymbol{x}_3^T \end{pmatrix} \begin{pmatrix} y_1/\|\boldsymbol{y}\| \\ y_2/\|\boldsymbol{y}\| \\ y_3/\|\boldsymbol{y}\| \end{pmatrix} = -\boldsymbol{P}\boldsymbol{X}\hat{\boldsymbol{y}}.$$

Similarly, the FDOA equations (8) can be put into matrix form

$$\boldsymbol{f} = -\boldsymbol{P}\boldsymbol{V}\hat{\boldsymbol{y}}, \tag{13}$$

where again $\boldsymbol{P}$ is a differencing matrix as above and $\boldsymbol{V} = (\boldsymbol{v}_1^T, \boldsymbol{v}_2^T, \ldots, \boldsymbol{v}_n^T)^T$.

We see from (12) and (13) that the far-field TDOA (respectively FDOA measurements) must lie in the image of the unit circle under transformation by $-\boldsymbol{P}\boldsymbol{X}$ (respectively $-\boldsymbol{P}\boldsymbol{V}$). This image is an ellipse with rotation and scaling that can be determined from the singular value decomposition of $\boldsymbol{P}\boldsymbol{X}$ (respectively $\boldsymbol{P}\boldsymbol{V}$). See Figure 8 for an example of such an ellipse for the FDOA case.

The least-squares estimate of the DOA $\hat{\boldsymbol{y}}$ can be calculated using the pseudoinverse for the associated systems (12) and (13):

$$\begin{aligned} \hat{\boldsymbol{y}} &= -\left[(\boldsymbol{P}\boldsymbol{X})^T\boldsymbol{P}\boldsymbol{X}\right]^{-1}(\boldsymbol{P}\boldsymbol{X})^T\boldsymbol{\tau} \qquad \text{(TDOA only)} \\ \hat{\boldsymbol{y}} &= -\left[(\boldsymbol{P}\boldsymbol{V})^T\boldsymbol{P}\boldsymbol{V}\right]^{-1}(\boldsymbol{P}\boldsymbol{V})^T\boldsymbol{f}. \qquad \text{(FDOA only)} \end{aligned} \tag{14}$$

The condition that the matrix $\boldsymbol{P}\boldsymbol{V}$ be nonsingular, which is needed for the second line of (14), corresponds to the requirement that the relative velocities of the receivers be nonzero (*i.e.,* the unequal velocity case). One benefit of this method for DOA calculation is that de-noising is automatically performed; this is because projection onto the range of $-\boldsymbol{P}\boldsymbol{X}$ (respectively $-\boldsymbol{P}\boldsymbol{V}$) is equivalent to projection onto the range of $\boldsymbol{P}$. Numerical tests for the FDOA DOA estimation approach and a comparison with the associated Cramér-Rao bound were carried out in [5], [24].

Clearly far-field TDOA and (unequal-velocity, far-field) FDOA measurements may be combined arbitrarily.

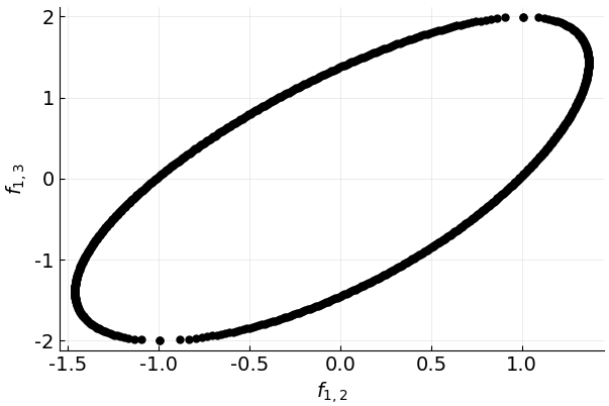

Fig. 8. Plot of far-field $f_{1,2}$ vs. $f_{1,3}$ for a system of three receivers centered around the origin. The image is an ellipse with scaling in the direction of the left singular vectors of $\widetilde{\boldsymbol{V}}$.

VI. Conclusion

The FDOA curves and surfaces are very complicated in the near field, but in the far field, we showed that they simplify dramatically to easily-understood curves and surfaces. In general, the equal-velocity FDOA surfaces are closed surfaces similar to a torus. The unequal-velocity FDOA surfaces become cones in the far field. In this latter case, having prior knowledge of the source altitude gives rise to FDOA hyperbolas on the constant-altitude plane, which extends a desirable quasi-near-field regime to a distance comparable to the sensor height.

We showed that in the case of unequal sensor velocities, the TDOA and FDOA curves and surfaces become tangent

in the far field. Consequently, attempts to find the range of a distant source from single-look multiple-FDOA or TDOA-FDOA measurements, using sensors with different velocities, are unlikely to succeed without aditional information.

The TDOA-FDOA situation is better in the known-altitude case, where the quasi-near-field region on the known-altitude plane extends laterally roughly to the same distance as the source altitude. In this region, TDOA and FDOA curves can intersect transversally.

In the far field, we gave a characterization of feasible TDOA and unequal-velocity FDOA measurements; this characterization depends only on the (assumed known) sensor positions and velocities. Far-field TDOA and unequal-velocity far-field FDOA measurements can be used to determine the source DOA by a simple pseudo-inverse linear formula, which automatically projects the measurements onto the feasible manifold. This method for obtaining DOA from far-field FDOA measurements was studied more thoroughly in the dissertation [5] and preprint [24].

We leave for the future the questions regarding 1) how to use far-field equal-velocity FDOA measurements to determine the source location and velocity and 2) how to understand and use the near-field FDOA measurements.

APPENDIX A
DERIVATIVE OF A UNIT VECTOR

$$\begin{aligned}\frac{\partial}{\partial z_i}\widehat{\boldsymbol{z}}^T\cdot\boldsymbol{v} &= \frac{\partial}{\partial z_i}\frac{\boldsymbol{z}^T\cdot\boldsymbol{v}}{\sqrt{\sum_j z_j^2}} = \frac{v_i}{\sqrt{\sum_j z_j^2}} - \frac{z_i(\boldsymbol{z}^T\cdot\boldsymbol{v})}{\left(\sqrt{\sum_j z_j^2}\right)^{3/2}}\\ &= \frac{v_i - (z_i/\|\boldsymbol{z}\|)(\widehat{\boldsymbol{z}}^T\cdot\boldsymbol{v})}{\|\boldsymbol{z}\|}.\end{aligned} \tag{15}$$

Consequently

$$\nabla_{\boldsymbol{z}}(\widehat{\boldsymbol{z}}^T\cdot\boldsymbol{v}) = \frac{I-\widehat{\boldsymbol{z}}\widehat{\boldsymbol{z}}^T}{\|\boldsymbol{z}\|}\cdot\boldsymbol{v}. \tag{16}$$

APPENDIX B
KNOWN ALTITUDE HYPERBOLAS

The TDOA and FDOA far-field cones are of the form

$$\widehat{\boldsymbol{y}}\cdot\boldsymbol{a} = d, \tag{17}$$

where the cone axis $\boldsymbol{a}$ is either the difference between the sensor locations or the difference between the velocities. For simplicity, we choose coordinates so that the cone axis is $\boldsymbol{a} = (a,0,0)$. For a source positioned at the point $\boldsymbol{y} = \boldsymbol{z}$, we have $d = \widehat{\boldsymbol{z}}\cdot\boldsymbol{a} = az_1/\|\boldsymbol{z}\|$. The intersection of (17) with the horizontal plane at $y_3 = h$ is easily found to be the hyperbola

$$\frac{a^2-d^2}{d^2h^2}y_1^2 - \frac{y_2^2}{h^2} = 1, \tag{18}$$

which, since the y_1^2/h^2 coefficient is

$$\frac{a^2-d^2}{d^2} = \frac{a^2}{d^2} - 1 = \frac{\|\boldsymbol{z}\|^2}{z_1^2} - 1 = \frac{\|\boldsymbol{z}\|^2 - z_1^2}{z_1^2}, \tag{19}$$

can be written

$$\frac{\left(\|\boldsymbol{z}\|^2 - z_1^2\right)}{z_1^2}\frac{y_1^2}{h^2} - \frac{y_2^2}{h^2} = 1. \tag{20}$$

The y_1-intercepts of the hyperbola are

$$y_1 = \frac{\pm hz_1}{\sqrt{\|\boldsymbol{z}\|^2 - z_1^2}} = \frac{\pm hz_1}{\sqrt{z_2^2+z_3^2}}. \tag{21}$$

Its foci are located at $(\pm c, 0, h)$, where

$$c = h\sqrt{\frac{z_1^2}{\|\boldsymbol{z}\|^2 - z_1^2} + 1} = \frac{h\|\boldsymbol{z}\|}{\sqrt{\|\boldsymbol{z}\|^2 - z_1^2}} = \frac{h\|\boldsymbol{z}\|}{\sqrt{z_2^2+z_3^2}}. \tag{22}$$

The coefficient of h in (22) depends on the source direction but in general is greater than 1.

ACKNOWLEDGMENT

The authors would like to thank Jim Given for helpful discussions. Any opinions, findings, and conclusions or recommendations expressed in this material are those of the authors and do not necessarily reflect the views of the United States Air Force or of the United States Navy.

REFERENCES

[1] K. C. Ho and Y. T. Chan, "Geolocation of a known altitude object from TDOA and FDOA measurements," *IEEE Transactions on Aerospace and Electronic Systems*, vol. 33, no. 3, pp. 770–783, July 1997.

[2] K. Ho and W. Xu, "An accurate algebraic solution for moving source location using TDOA and FDOA measurements," *IEEE Transactions on Signal Processing*, vol. 52, no. 9, pp. 2453–2463, 2004.

[3] K. Ho, X. Lu, and L.-o. Kovavisaruch, "Source localization using TDOA and FDOA measurements in the presence of receiver location errors: Analysis and solution," *IEEE Transactions on Signal Processing*, vol. 55, no. 2, pp. 684–696, 2007.

[4] K. J. Cameron and D. J. Bates, "Geolocation with FDOA measurements via polynomial systems and RANSAC," in *2018 IEEE Radar Conference (RadarConf18)*, April 2018, pp. 0676–0681.

[5] K. J. Cameron, "FDOA-based passive source localization: a geometric perspective," Ph.D. dissertation, Colorado State University. Libraries, 2018.

[6] A. Amar and A. J. Weiss, "Direct position determination: A single-step emitter localization approach," in *Classical and modern direction-of-arrival estimation*. Elsevier, 2009, pp. 385–424.

[7] A. J. Weiss and A. Amar, "Direct geolocation of stationary wideband radio signal based on time delays and doppler shifts," in *2009 IEEE/SP 15th Workshop on Statistical Signal Processing*. IEEE, 2009, pp. 101–104.

[8] A. J. Weiss, "Direct geolocation of wideband emitters based on delay and doppler," *IEEE Transactions on Signal Processing*, vol. 59, no. 6, pp. 2513–2521, 2011.

[9] M. Cheney and J. A. Given, "Wideband passive source localization," *Inverse Problems*, vol. 33, no. 8, p. 085007, 2017. [Online]. Available: http://stacks.iop.org/0266-5611/33/i=8/a=085007

[10] C. Waddington, M. Cheney, and J. A. Given, "Synthetic aperture source localization," *Inverse Problems*, vol. 36, no. 1, p. 015007, 2019.

[11] M. Compagnoni, R. Notari, F. Antonacci, and A. Sarti, "A comprehensive analysis of the geometry of TDOA maps in localization problems," *Inverse Problems*, vol. 30, no. 3, 2014.

[12] R. Schmidt, "Least squares range difference location," *IEEE Transactions on Aerospace and Electronic Systems*, vol. 32, no. 1, pp. 234–242, Jan 1996.

[13] R. O. Schmidt, "A new approach to geometry of range difference location," *IEEE Transactions on Aerospace and Electronic Systems*, vol. AES-8, no. 6, pp. 821–835, Nov 1972.

[14] J. Benesty, *Direction-of-Arrival and Time-Difference-of-Arrival Estimation*. Berlin, Heidelberg: Springer Berlin Heidelberg, 2008, pp. 181–215. [Online]. Available: https://doi.org/10.1007/978-3-540-78612-2_9

[15] D. J. Torrieri, "Statistical theory of passive location systems," *IEEE Transactions on Aerospace and Electronic Systems*, vol. AES-20, no. 2, pp. 183–198, March 1984.

[16] M. Cheney and B. Borden, *Fundamentals of Radar Imaging*. Society for Industrial and Applied Mathematics, 2009. [Online]. Available: http://epubs.siam.org/doi/abs/10.1137/1.9780898719291

[17] J. Li, X. Sun, P. Huang, and J. Pang, "Performance analysis of active target localization using TDOA and FDOA measurements in WSN," in *22nd International Conference on Advanced Information Networking and Applications-Workshops (aina workshops 2008)*. IEEE, 2008, pp. 585–589.

[18] J. Vesely, "Differential doppler target position fix computing methods," in *Proc. Int. Conf. Circuits, Syst., Signals*, 2010, pp. 284–287.

[19] P. Ellis, D. Van Rheeden, and F. Dowla, "Use of doppler and doppler rate for RF geolocation using a single LEO satellite," *IEEE Access*, vol. 8, pp. 12 907–12 920, 2020.

[20] W. d. C. Rodrigues and J. A. Apolinário, "An on-the-fly FDOA-based target localization system," in *2020 IEEE 11th Latin American Symposium on Circuits & Systems (LASCAS)*. IEEE, 2020, pp. 1–4.

[21] Y. Wang and K. Ho, "Unified near-field and far-field localization for AOA and hybrid AOA-TDOA positionings," *IEEE Transactions on Wireless Communications*, vol. 17, no. 2, pp. 1242–1254, 2017.

[22] S. R. Drake and K. Dogancay, "Geolocation by time difference of arrival using hyperbolic asymptotes," in *2004 IEEE International Conference on Acoustics, Speech, and Signal Processing*, vol. 2, May 2004, pp. ii–361–4 vol.2.

[23] X. Sun, J. Li, P. Huang, and J. Pang, "Total least-squares solution of active target localization using TDOA and FDOA measurements in WSN," in *22nd International Conference on Advanced Information Networking and Applications-Workshops (aina workshops 2008)*. IEEE, 2008, pp. 995–999.

[24] K. J. Cameron and S. J. Pine. (2018) A novel method for determining DOA from far-field TDOA or FDOA. arXiv:1808.04741. [Online]. Available: arXiv:1808.04741

[25] Y. Wang and Y. Wu, "An efficient semidefinite relaxation algorithm for moving source localization using TDOA and FDOA measurements," *IEEE communications Letters*, vol. 21, no. 1, pp. 80–83, 2016.

[26] M. Compagnoni, A. Canclini, P. Bestagini, F. Antonacci, A. Sarti, and S. Tubaro, "Source localization and denoising: a perspective from the TDOA space," *Multidimensional Systems and Signal Processing*, vol. 28, no. 4, pp. 1283–1308, Oct 2017. [Online]. Available: https://doi.org/10.1007/s11045-016-0400-9

Karleigh Cameron Pine received the B.S. degree in applied mathematics (2014) from Central Michigan University, the M.S. in applied mathematics (2016) and Ph.D. in mathematics (2018) from Colorado State University. Her research interests include polynomial systems, modeling of spatial-temporal networks, and autonomy. She is now a researcher at Matrix Research, Inc. in Dayton, Ohio.

Samuel Pine received the B.A. degree in mathematics and economics from Elmira College in 2014, the M.S. in applied mathematics from Colorado State University in 2016, and the Ph.D. in mathematics from Colorado State University in 2018. He is now a member of the RF Signals processing group at Matrix Research, Inc. in Dayton, Ohio.

Margaret Cheney received the B.A. degree in mathematics and physics from Oberlin College in 1976, and the Ph.D. in mathematics from Indiana University in 1982. She previously held positions at Stanford University (postdoc 1982-1984), Duke University (assistant prof., 1986-1988) and Rensselaer Polytechnic Institute (associate prof. 1988-1993 and prof. 1993-2012), and since 2012 has been the Albert C. Yates Endowment Professor of Mathematics at Colorado State University, where she also holds an appointment in the Department of Electrical & Computer Engineering. She has held visiting appointments at a variety of government laboratories.

She has published more than 70 refereed articles in international journals, together with a similar number of conference proceedings papers and reports. She co-authored the monograph Fundamentals of Radar Imaging, published by SIAM. She has given about 200 invited lectures all over the US and Europe. She holds 5 patents. She is a Fellow of the Institute of Physics and a Fellow of SIAM, and she was awarded an Honorary Doctor of Science by Oberlin College in 2011. She served 3 terms on the SIAM board of Trustees, and for the last 20 years has served on various SIAM committees. She has served on the editorial boards of five journals. Most of her work has been on the inverse problems that arise in acoustics and electromagnetics; since 2001, she has mainly been working on radar imaging.